The International Scientific and Technical Organization for Gliding

OSTIV MET PANEL 2019

7-8 March 2019, Goethe University Frankfurt, GERMANY

Geozentrum
3.101; In the third floor of the Geosciences Building

COLLOBORATION WITH

GOETHE UNIVERSITÄT FRANKFURT AM MAIN

EURAS Avrasya Üniversiteler Birliği Eurasian Universities Union

Goethe University of Frankfurt **Akaflieg Frankfurt** **Istanbul Aydın University**

OSTIV/ISTUS History

An early realization of the attractive possibility for meteorologists to learn more about the structure and behaviour of the atmosphere when using sailplanes, combined with the interest of aerodynamicists, aircraft- and instrument designers, constructors and pilots for improving sailplane performance and characteristics, lead in 1930 to the forming of the first international soaring organization ISTUS (Internationale Studienkommission für den motorlosen Flug).

Having as objective the furtherance of development of soaring in science and technics as well as in sports by "exchanging experience and friendly cooperation among the specialists and pilots of all nations engaged in soaring", this objective has been changed after World War II on occasion of forming OSTIV as the successor of ISTUS in July 1948 at Samedan / Switzerland. All the sporting objectives were separated from OSTIV and were integrated within the responsibility of the Fédération Aéronautique Internationale (FAI).

The new constitution of OSTIV concentrated merely to the objectives" to encourage and coordinate internationally the science and technology of soaring and the development and use of the sailplane in pure and applied research". After years of discussion OSTIV finally found its place as an International Associate Member of FAI (Resolution of the FAI General Conference at Rome, 4 October 1977); each party having the right of representation - with voting right - in the General Conferences of the other party. Furthermore, OSTIV has the right to delegate observers to the meetings of the International Gliding Commission (IGC) and vice versa and to delegate observers to the Sailplane Development-, Meteorological- and Training and Safety Panel-Meetings of OSTIV.

A most important decision, which FAI laid down in its rules, was the acceptance of offers for world soaring championships only under the condition that they assure simultaneously the organization of OSTIV-Congresses at the same time and place as the championships.

OSTIV MET PANEL 2019

7-8 March 2019, Goethe University Frankfurt, GERMANY

Geozentrum/3.101; In the third floor of the Geosciences Building

7 March 2019

09.00-09.30: REGISTRATION

Goethe University of Frankfurt, GERMANY

9.30 – 10.00	**7 March 2019** **OPENING SESSION & WELCOME SPEECH** **Joachim CURTIUS,** **Atmosphere Physics, Goethe University Frankfurt** **Christof MAUL, Akaflieg Frankfurt, Technische Universität Braunschweig** **Zafer ASLAN, Chair, OSTIV MET PANEL, Istanbul Aydın University, Istanbul, Turkey**
SESSION 1 THERMALS **Chair: Carsten LINDEMANN**	
10.00 - 10.30	**Thermals – a mystery uncovered** **Henry BLUM**
10.30 - 11.00	**Glider based Measurements in German Thermals** **Albert KIEßLING**
11.00-11.30	**COFFEE & TEA BREAK/POSTER SESSIONS**

SESSION 1 THERMALS **Chair: Henry BLUM**	
11.30 - 12.00	**Correct interpretation of glider in-flight environmental sensing in thermal updrafts** **Oliver PREDELLI, Ronald NIEDERHAGEN**
12.00-12.30	**Measuring the fine structures of thermals** **Alfed ULTSCH, Christof MAUL**
12.30-12.45 General Evaluation of Session 1 THERMALS **Henry BLUM, Carsten LINDEMANN**	
12.45-14.00	**LUNCH**
SESSION 2 WAVES **Chair: Dietr ETLING**	
14.00-14.30	**Some Common Features of Thermal Waves** **Carsten LINDEMANN**
14.30-15.00	**The turbulence and wind shear effects of wind turbines** **Rene HEISE**
15.00-15.30	**COFFEE & TEA BREAK / POSTER SESSIONS**
SESSION 2 WAVES **Chair: Rene HEISE**	
15.30-16.00	**Diagnostics of Turbulence and Mountain Wave Generation in Aviation Forecasting at the Hungarian Meteorological Service** **Péter SALAVEC, André SIMON, Balázs SZINTAI**
16:00-16.30	**Trapped and Vertically Propagating Waves** **Timothy CHOW**
16.30-16.45 General Evaluation of Session 2 WAVES **Christof MAUL, Rene HEISE**	

8 March 2019 SESSION 3 OSTIV MET PANEL Joint Training Activities, Co-operations Chair: Christof MAUL	
09:30 - 10.00	Discussion on training programs, documentaries, web pages
10:00 - 10.30	Special Applications of Model Output Statistics (MOS) in Operational Weather Forecasting Bernd RICHTER
10.30 - 10.45 Christof MAUL	Evaluation of Session 3
11.00-11.30	COFFEE & TEA BREAK
SESSION 4 OSTIV MET PANEL Joint Research Activities, Co-operations Chair: Joachim CURTIUS	
11.30 - 12.30	Discussion on joint research programs, applications, supports
12.30-12.45 Joachim CURTIUS	Evaluation of Session 3
12.45-13.00 General Evaluation of OSTIV Met Panel / Closing Session Zafer ASLAN, Christof MAUL	

Host Institution: Goethe University of Frankfurt

In collaboration with:

*Prof. Dr. Alfred Ultsch, **University of Marburg**, ultsch@Mathematik.Uni-Marburg.de*

*Prof. Dr. Joachim Curtius, Atmosphere Physics, **Goethe University of Frankfurt,** Geocenter, Altenhöferallee 1, University of Frankfurt Campus Riedberg, curtius@iau.uni-frankfurt.de*

*PD. Dr. Christof MAUL, **Akaflieg Frankfurt, Technische Universität Braunschweig,** Germany c.maul@tu-braunschweig.de*

*Prof. Dr. Zafer Aslan, Chair; OSTIV MET PANEL, **Istanbul Aydın University,** zaferaslan@aydin.edu.tr, https://www.aydin.edu.tr*

*Pınar Elbasan, **EURAS, Eurasian Universities Union;** pinarelbasan@aydin.edu.tr, https://euras-edu.org/*

For Accommodation

Relexa, https://www.relexa-hotel-frankfurt.de/ that is 5 minutes' walk from the conference site: Room 3.101 at Geozentrum, Altenhöferallee 1, Campus Riedberg, and close to public transportation: U-Bahn-Line U2; stop: Riedwiese/Mertonviertel

Dinner:

07 March 2019; Thursday evening (19.00)

"Lahmer Esel" restaurant (https://lahmer-esel.de/) which is a traditional Frankfurt style pub and restaurant. It is in walking distance (less than 10 minutes) from the campus.

OSTIV MET PANEL (7-8 March 2019)
Participant List

No	Name-Surname	e-mail	Country
1	Albert KIEßLING	albert.kiessling@t-onlilne.de	Germany
2	Alfred ULTSCH,	ultsch@Mathematik.Uni-Marburg.de	Germany
3	André SIMON		
4	Balázs SZINTAI		
5	Bernd RICHTER	bernd.richter@web.de	Germany
6	Carsten LINDEMANN	carstenl@zedat.fu-berlin.de	Germany
7	Christof MAUL	c.maul@tu-braunschweig.de	Akaflieg Frankfurt, Technische Universität Braunschweig, Germany
8	Dietr ETLING	etling@muk.uni-hannover.de	Germany
9	Gökhan ERDEMIR	gokhan.erdemir@izu.edu.tr	ISZU, Turkey
10	Henry BLUM	henry.blum@gmx.net	Germany
11	Ines WEBER	weber.ines@gmx.net	Akaflieg Munich Germany
12	Joachim CURTIUS	curtius@iau.uni-frankfurt.de	Atmosphere Physics, Goethe University Frankfurt, Germany
13	Oliver PREDELLI	oliver.predelli@freenet.de	Germany
14	Péter SALAVEC	salavec.p@met.hu	Hungary
15	Rene HEISE	Rene.Heise@t-online.de	Germany
16	Ronald NIEDERHAGEN	ronald_niederhagen@freenet.de	Germany
17	Thomas SEILER	thomas.seiler@lat.dlh.de	Germany
18	Timothy CHOW	tim_chow@hotmail.com	USA
19	Zafer ASLAN	zaferaslan@aydin.edu.tr	Istanbul Aydın University, Istanbul, Turkey

Glider based Measurements in German Thermals

Albert Kießling

Akademische Fliegergruppe am Karlsruher Institut für Technologie e. V, Germany, albert.kiessling@t-online.de

Abstract

Based on my measurements made over the Namibian steppe in the year 2017, which were presented and published during the OSTIV Met session at Příbram 3. August 2018, adequate measurements were pursued during the gliding season of the last year over Southern Germany. This time, the measurements were taken from a new optimized sensor assembly mounted on the total energy tube at the vertical tail of my 18m class glider. The sensor is - due to the special sensor housing and the mounting position - able to measure the 3 thermal parameters pressure, temperature and humidity, largely unaffected by the solar radiation and the velocity of the glider. The construction of the sensor assembly is roughly described in order to exclude the typical measuring doubts.

Again, the main goal of the measurements was to detect the influence of temperature and humidity on the thermals and to compare the measurements with the results taken in the Namibian steppe. The raw data have been analyzed by means of calculating the potential temperature inside and outside of the thermals, principally assuming, that the surrounding atmosphere is stratified neutral during the convection time. Additionally the vertical temperature and humidity profiles in single thermals could be extracted from the measured flight data and are presented in diagrams similar to the well-known Temps. Specific influences of the surface structures like mountains and small valleys have been discovered more or less randomly and will be discussed as well.

***Keywords*:** Buoyancy factor, warm air thermals, temperature and humiditiy difference, flight track measurements, potential temperature

Introduction

A lot of modern glider instruments offer the direct indication of the potential temperature during the flight and some pilots use that indication as an aid to center or to find the thermals. The used temperature sensors mostly are located in the ventilation tube near the nose of the glider, where the temperature is influenced by pressure variations combined with velocity variations, which themselves cause adiabatic temperature deviations dependent from the velocity of the glider and the air ventilation inside the cockpit. But much more relevant is the long response time of those temperature sensors (~ 10s to 20s), which cause big measurement errors depending on the climbing or sinking rate of the glider. The following diagram in figure 1 shows this relationship for a sensor with a response time of only 4s. Correspondingly, the much longer response times of typical sensors cause much higher temperature errors.

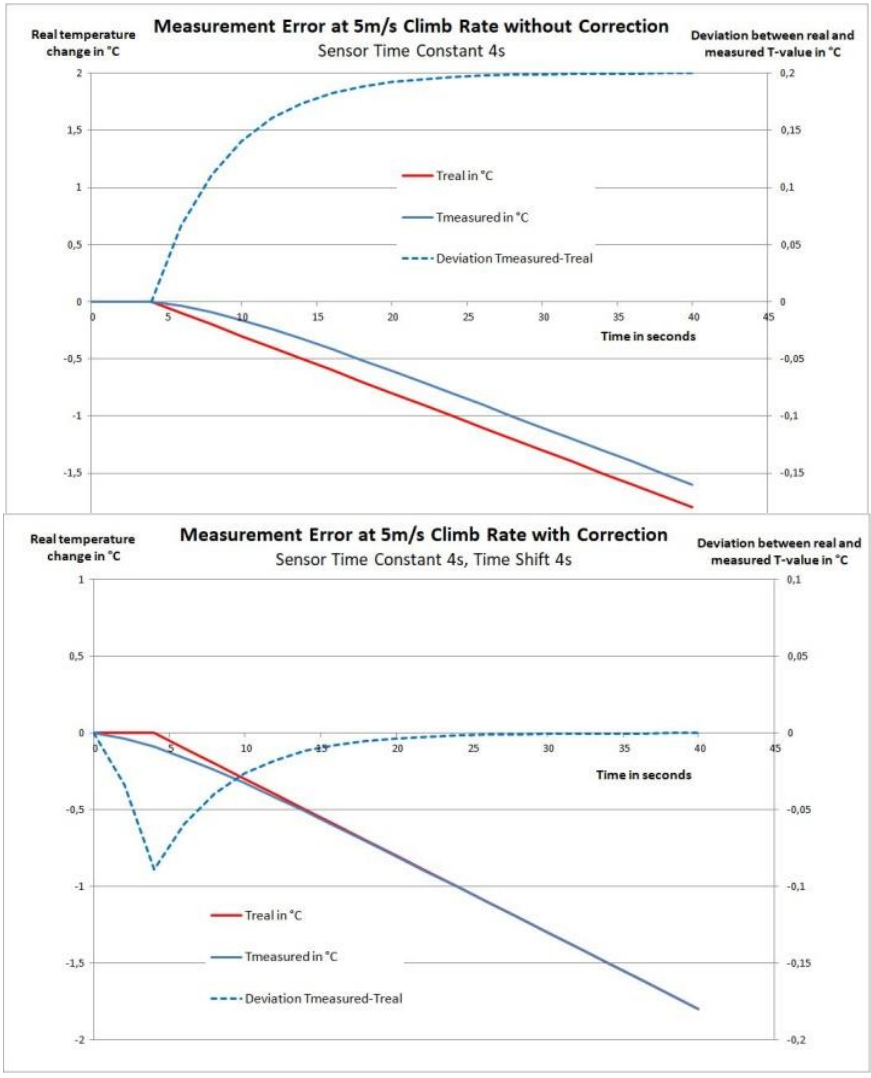

Figure 1: Measurement errors of temperature sensors with a response time of 4 seconds at 5 m/s climbing rate with and without correction

The above presented logger takes all 2 seconds samples of the measured temperature, so the real temperature can be relatively simple approximated by shifting the sampled data by 2 sampling periods as shown on the right side of figure 1. The so processed temperature can be easily compared with the temperature of the surrounding – adiabatic stratified - air based on the measured pressure/altitude signal, which has a response time of only some milliseconds. The corrected temperature values can therefore be used to calculate the potential temperature with a maximum residual error of only 0,08°C.

Construction of the used PTH-Sensor

The PTH-sensor is based on two precise semiconductor sensors, one of the chips measures the static pressure and the second one the temperature and the humidity together. Both sensors are assembled on a planar PCB- (printed circuit board) sandwich. The batterypowered data logger is based on a consumer product, which has been modified in order to locate the sensor separately from the logger. The temperature chip is arranged in a spider net out of thin copper wires in order to get low response times (see figure 2 right). Additionally the chip has to be well ventilated by an airflow, which does not produce speed dependent adiabatic temperature variations. Both have been guaranteed by the well-shaped housing, which has been tested in a lot of flights at speeds between 90 to 240km/h.

Figure 2: Planar PTH-sensor fixed to the compensation tube and arrangement of the TH-sensor in the PCB-sandwich

Measuring Method

The first method to judge the influence of the temperature difference between inside and outside the thermals is to calculate the potential temperatures based on the measured temperature and the measured static pressure, assuming, that the adiabatic lapse rate of the surrounding atmosphere is 1°C/100m. If the potential temperature during the circling is increased, this increase corresponds directly to the temperature difference between inside and outside of the thermals and matches directly to the thermal buoyancy factor. The influence of the humidity can immediately be read out of the measured mixture ratio in g water vapour / kg air by means of the following approximation: 6 g/kg difference between inside and outside the thermals corresponds to about 1°C temperature difference, which is usually called the virtual temperature difference. That virtual temperature difference can directly be compared with the thermal temperature difference and hence interpreted as the buoyancy factor of the humidity. This method has to take into account, that the potential temperature over the whole flight slowly increases with the ongoing daytime as well as with the surface structure of the landscape (see figure 3a).

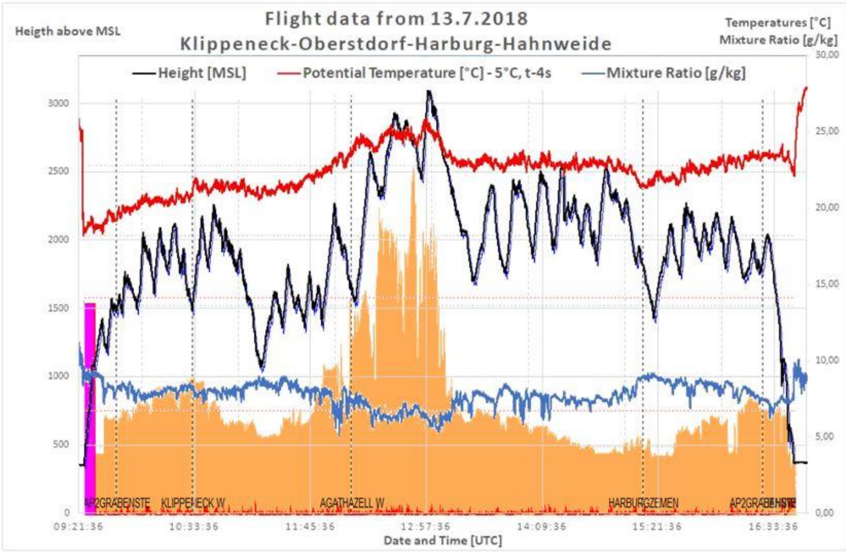

Figure 3a: Flight documentation with depicted surface profile of the Swabian Alb and the Bavarian Alps

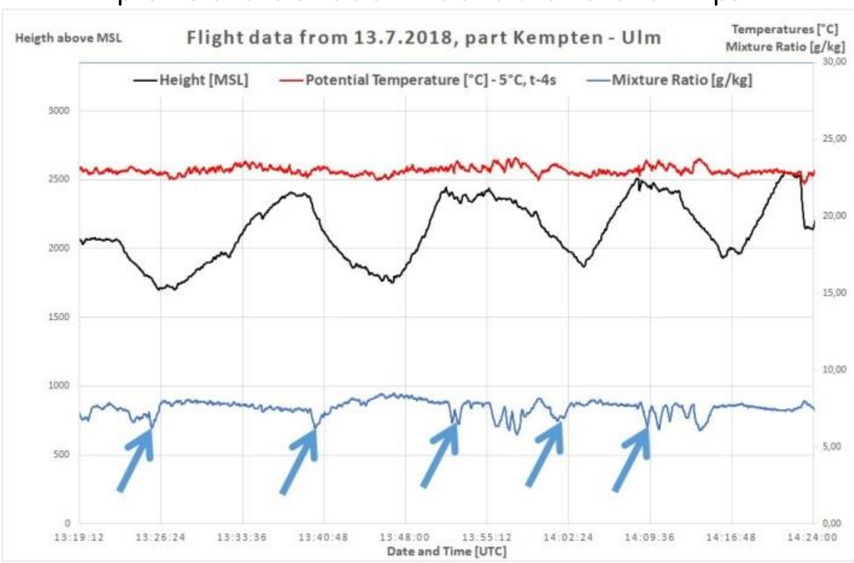

Figure 3b: Zoomed part with dry zones around the thermals (see arrows)

The second method is able to generate vertical temperature and humidity profiles similar to the well known Temp-diagrams. In this case, the temperature and humidity profiles have to be extracted manually from the measured PTH-data separated by a section from inside the regarded thermal and a section from the surrounding air. Optionally the values can be extracted from the surrounding air before or after the climbing in the thermal. However, the result is similar. The accuracy of this method is on one hand dependent from the skills of the pilot to climb in the center of the thermal and on the other hand, from the track, the glider has taken before or after the circling (see figures 4).

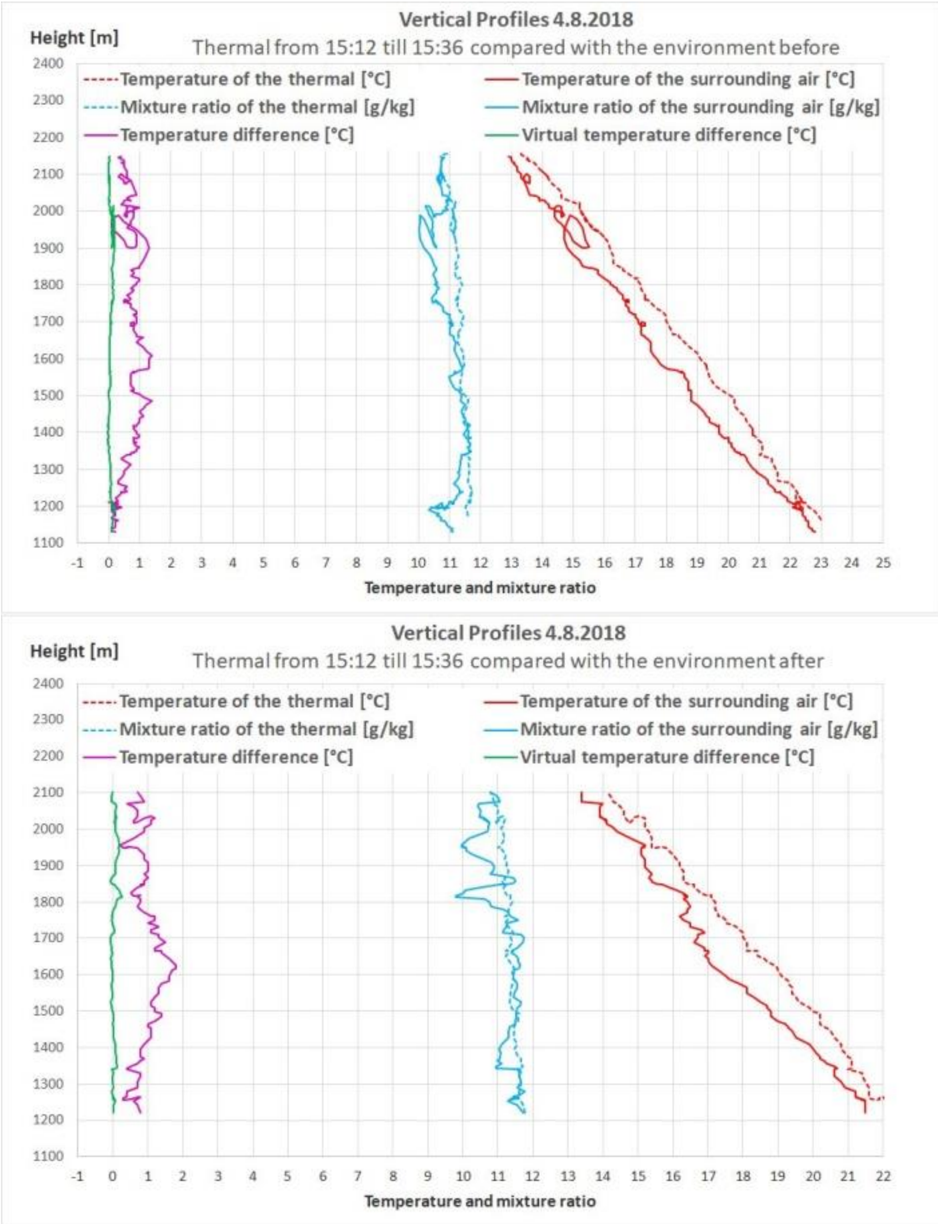

Figure 4: Vertical profiles of a thermal compared with the data from the glide track before and after the circling

To minimize the "track" errors, the ascents in the thermal and the descents in the surrounding air were made cloth together without touching other thermals (see the profiles in figure 5). Additionally these ascents and descents were made several times at nearly the same location in order to get comparable results.

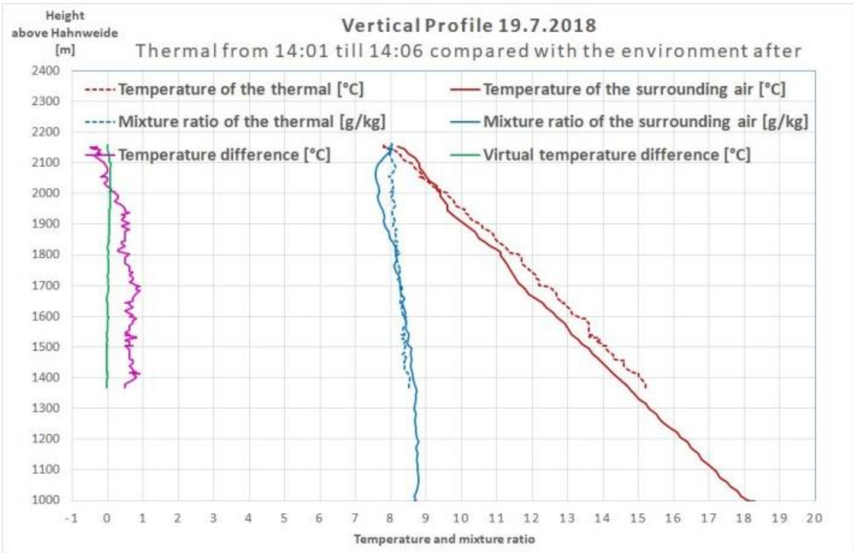

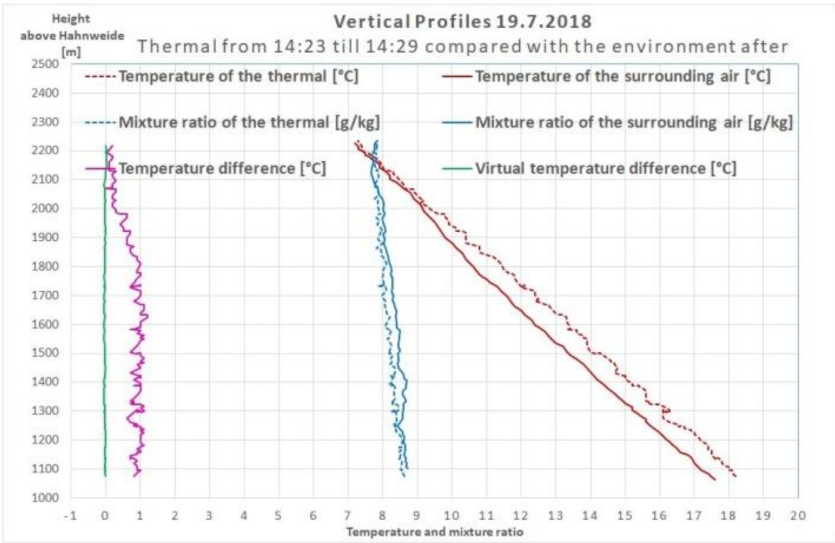

Figure 5: Vertical profiles of thermals, where the environment values are taken from the airbrake-supported descent in the immediate vicinity of the thermal.

Results

Although the cloud base in Germany usually is lower and respectively the total humidity is higher than in Namibia, the contribution of the humidity buoyancy is similarly low as in the dry air of Namibia. All 4 diagrams in figure 4 and 5 show a clear dominating influence of the thermal buoyancy. But there are - like in Namibia - some cases of dry air flowing down from higher regions, especially if the thermals penetrate into subsiding inversions as shown in my first paper (see reference 1). The dry regions nearby the thermals can easily be seen in the zoomed horizontal diagram of figure 3b. In this case, the humidity buoyancy can help the thermals to climb further on, even in cases, where the thermal buoyancy is going negative as shown in the vertical profiles of figure 5 left.

Some special phenomena could be extracted out of the measured data. For example, the vertical profiles of figure 5 show, that the air inside the thermals is sometimes - on lower levels - drier than the surrounding air. The thermals have obviously been generated over dry areas, where the evaporation of humidity takes less energy from the solar radiation than over humid ones, why it doesn’t seem a good idea to look for humid areas to find good thermals.

As already mentioned above, the influence of the landscape in Germany seems to be greater than in the homogeneous Namibian steppe. The following figures 6 and 7 show for example the influence on the horizontal humidity and potential temperature distribution: When crossing small valleys of the Swabian Alb aligned in the direction of the local wind - which can be estimated from the horizontal displacement during the circling phases in figure 6 - the humidity is falling down over the valleys and the potential temperature increases slightly at the same time. Above valleys, which lie perpendicular to the wind direction, there are no humidity and temperature variations observed. An explanation for the phenomena could be, that the wind blows drier and warmer air masses from outside the hills along the valleys into the higher regions of the Swabian Alb. It would be interesting if similar effects could be detected in the bigger valleys of the Alps.

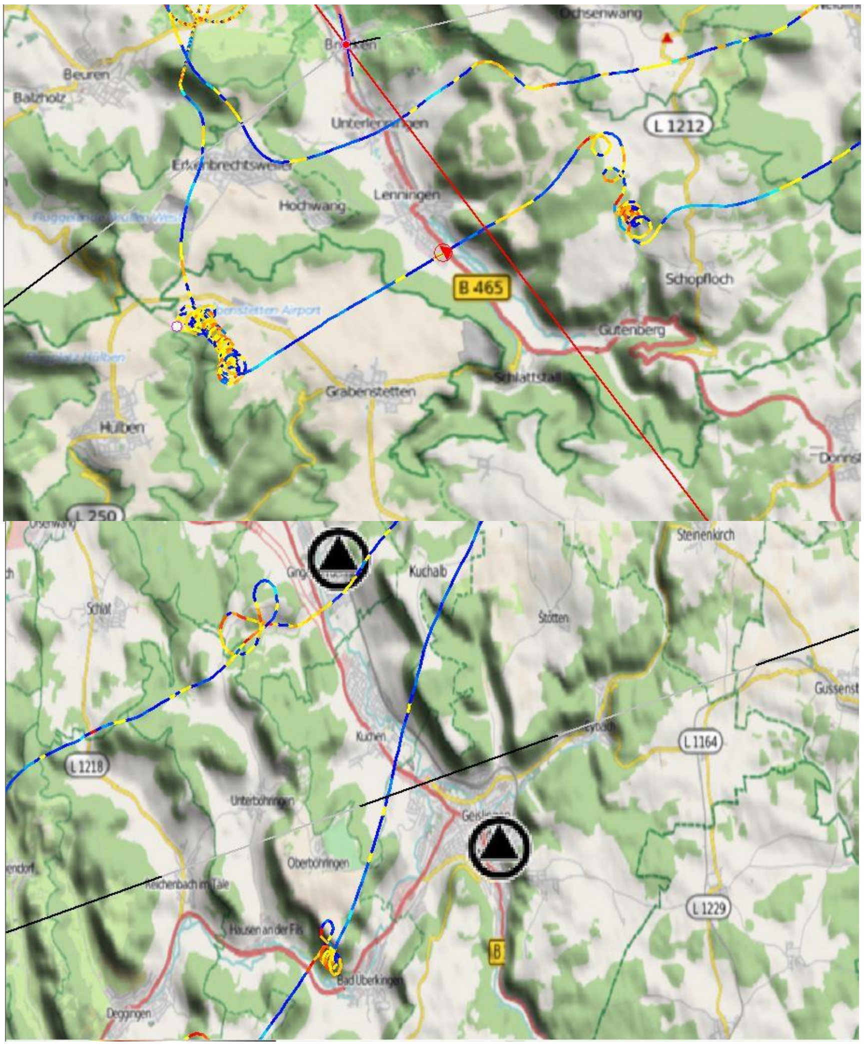

Figure 6: Crossing the Lenningen valley (left) and the Fils valley (right), the wind is blowing along the valleys

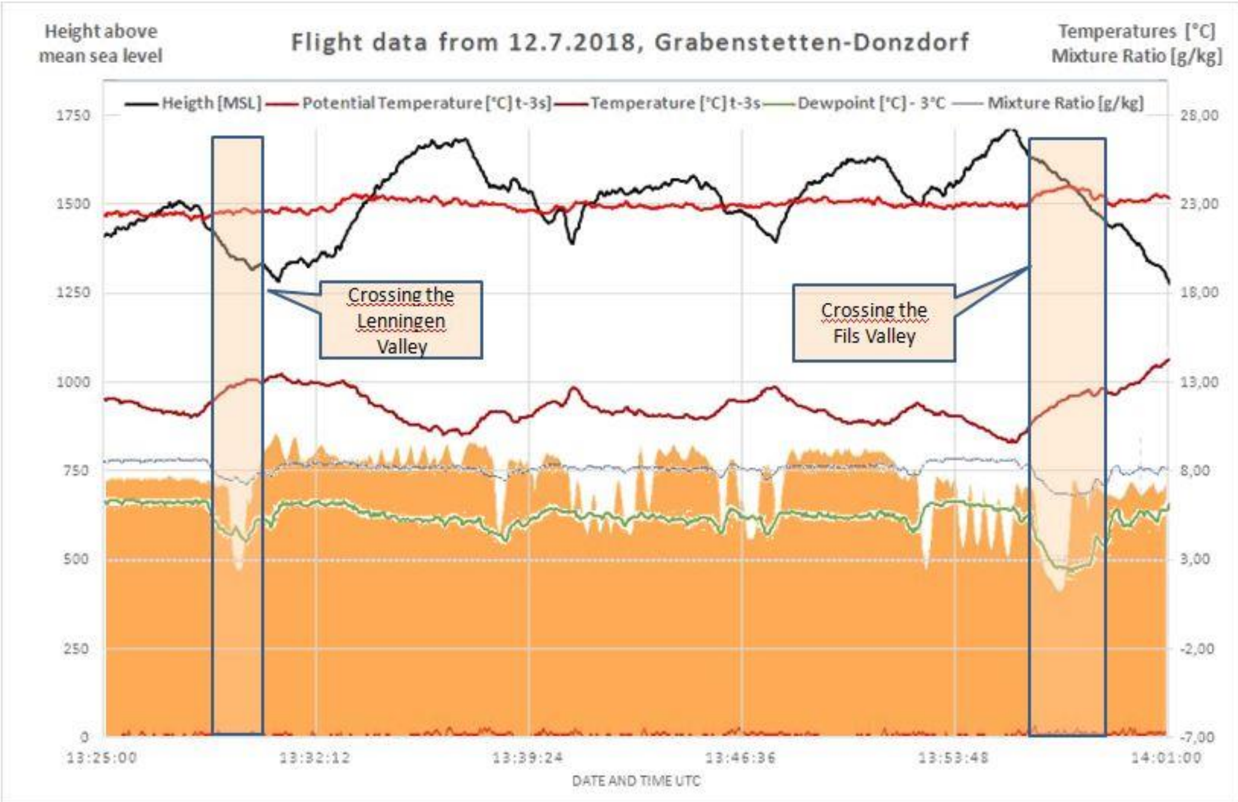

Figure 7: Crossing the Lenningen and Fils valleys shows noticeable effects on the humidity or on the potential temperature

Conclusion

German thermals show similar regularities as Namibian ones and are mainly driven by thermal buoyancy (temperature difference to the surrounding air), the effective height of which is not a fixed value as sometimes supposed. The height of thermal buoyancy can be estimated to be 200 to 300m less than the convection height, which due to this dependency serves as a general quality reference. Simply expressed: Namibian thermals are only better than German ones if their cloud base is higher. Humidity supports the thermal buoyancy only in a few cases near the cloud base.

Acknowledgement
I would like to thank to Olivier Liechti for the precious inputs and the active support in the preparation of the data and to

Hermann Trimmel for his suggestions and final corrections.

References

[1]Albert Kießling, extended abstract of the XXXIV OSTIV Congress Příbram, Czech Republic 29 July – 3 August, 2018

Correct interpretation of glider in-flight environmental sensing in thermal updrafts

Oliver Predelli, Ronald Niederhagen

This paper describes the most significant sources of errors and disturbance when measuring temperature and humidity with a glider. Measurement flights have been started from different airports in Germany, between April and August of 2018, resulting in a collection of over 90 hours of flight data logs. We show how error correction can be applied to the measurement data. Analysis of the data indicates that core assumptions of the theories of thermals, which have been published for decades, cannot be backed up by our measurement data. In contrast, we present a revised view of temperature and humidity inside thermals. As a result, traditional understanding of temperature distribution and entertainment processes must be revised.

Introduction

Mobile Devices and Internet of Things (IoT) have triggered a strong investment in sensor technology (Micro-Electro-Mechanical Systems, MEMS) and small portable computer devices (SoC). Over the past decade, this investment has led to significant quality improvements as well as cost reduction. It is straightforward to use this equipment in a glider to measure air temperature, humidity and air pressure. Gliders are especially suitable for detailed analysis of thermals because they naturally use thermals flying at low speeds in tight circles.

Nevertheless measuring air temperature and humidity in flight is nontrivial. There are many sources of errors and mistakes, which have to be considered in order to understand the validity of the data. Examples of such errors include the heat capacity of the glider's fuselage, which may impact the temperature of the air around it. Or a "dry offset" for humidity sensors which were not designed for high airspeed. Also the result of a water-to-air mixing ratio calculation will be wrong if the temperature measurement was erroneous in the first place. A detailed understanding of the causes to these errors is the basis for developing error correction algorithms. They can be used to eliminate errors in a post-process after the data acquisition. Ignoring these erroneous effects may result in faulty interpretation of the data. Several attempts of former in-flight data acquisition suffer from that.

In-flight measuring equipment

A sensor of type BME280 from Bosch Sensortec [BME280] is used to sample humidity, pressure and temperature data. The sensor is operated from a dedicated micro controller, which records the data from the BME280 together with a GPS-based timestamp. The data from the glider's flight and navigation instruments are recorded in a separate unit also together with a GPS-based timestamp. Both units' sample rate is 2 Hz. After the flight, the two recorded data streams are synchronized - by means of the GPS-based timestamps - merged together and the result is written to a CSV-File containing one data vector for every half second. The data vector includes humidity, pressure and temperature, as well as Pstat, Ppitot, Pte, GPS-fix, course, TE-vario and airspeed.

It is important to pick the optimal position for the environmental sensors. Unpredictable influences must be avoided or at least minimized and systematic influences must be modeled to allow for data correction in the post-process. Systematic influences include variation in airspeed, influences of parasitic heat capacity upstream or around the sensor, or heat radiation from the sun.
Unpredictable influences include turbulent airflow around the sensor or yawing of the glider, which changes the airflow around the sensor as the alignment changes between the glider's roll axis and the glider's motion vector. Thus, the sensor may be exposed to either fresh air or air, which has flown over the surface of the glider.

For the data acquisition of this publication, the sensor was positioned inside the ventilation channel to the cockpit of the glider. Thus it is protected from direct sunlight and the misalignment of the glider's roll axis has nearly no effect.

Temperature correction

The result of the effects mentioned above is that the measured temperature suffers from a time lag relative to the temperature of interest. On falling air temperature (during ascend) the sensor reads a slightly warmer temperature. Whereas in rising air temperature (during descend) the reading is slightly colder. Plotting altitude over temperature exhibits a more or less distinct loop form, very much like a hysteresis curve. There are some older publications, which interpret this loop form as a temperature difference between the thermal and the ambient air with increased potential temperature during ascent and reduced potential temperature during descent. One example where the loop form becomes apparent is the tow phase. During that phase, the tow plane pulls the glider to the release point. Typically, this is an ascent outside of thermals. There should be no increase of the potential temperature under these conditions. If it was, a time lag was influencing the temperature measurement.

The most noticeable influence on the sensor's operation is caused by the presence of heat capacitance upstream from the sensor and the heat capacitance of the sensor package and fixture itself. Heat conduction in this system can be modeled by a 2nd order low pass filter. The first time constant reflecting the heat capacitance in the channel. In our case, 80 sec were determined for that. The second time constant reflecting the package and the fixture of the sensor being 5 sec. These two parameters have been determined in lab experiments and have been verified by correlation of nearly 100 hours of flight data records.

However, it turns out that the second time constant can be safely ignored as it has only a minor impact on the calculation. This simplifies the correction algorithm.

The recorded data is post-processed such that the temperature in the undisturbed air immediately in front of the glider's nose is available for subsequent calculation. The temperature error can be estimated by comparing a simulated measurement temperature based on a dry adiabatic lapse rate with the actual measurement temperature. The parameters of the simulation model are tuned to achieve maximum correlation between simulation and measurements for all flights and all phases. The accuracy of the calculated temperature has been demonstrated to typically lie within a range of less than +/- 0.1 K of the true value.

It is important to note that the applied data correction does not depend on the altitude nor does it imply any form of dry-adiabatic lapse rate.

Humidity correction

The in-flight measurements show that the humidity sensor of the BME280 exhibits a "dry offset". That means that the relative humidity is always too low resulting in a calculated dew point temperature, which is ~ 2.5 °C lower than expected. This dry offset can only be observed in flight. When standing still on the ground or in the lab the dew point values correspond to the values published by the German Weather Service (DWD) for that place and time. We assume the dry offset has to do with the speed at which the air passes by the sensor. The BME280 may not have been designed for such conditions although the data sheet is not explicit about that.

One possible and plausible explanation for the dry offset behavior under those conditions can be related to the measurement principle of the sensor. A thin layer of water builds on the surface of such solid-state capacitive moisture sensors [And94]. This water film is a few molecule diameters thick and caused by adsorption. The thickness depends on the relative humidity and the temperature of the measured air and represents the measurement principle of this sensor type.

As pointed out in [And94] the strong airflow around the sensor may cause a reduction in thickness of the adsorbed water film. This leads to afore mentioned dry offset and the lower than expected humidity values from the sensor.

Considering Van-Der-Waals-Forces we correct the thickness of the water layer thus correcting the relative humidity values. As with the temperature correction, also the humidity correction is independent of the particular flight or any other parameter, so that the same algorithm can be applied to correct all acquired data.

Results

Fig. 1 shows the results of a flight on May 14, 2018. The plot uses a format, which is widely used for thermodynamics diagrams. The dotted line shows the uncorrected temperature values exhibiting afore mentioned loop form. The solid curve on the right shows the corrected temperature. The left solid curve shows the dew-point temperature. Letters denote significant time points during the flight, which include: the end of the tow phase after takeoff, searching and circling in the first thermal, cruising to the next thermal. The embedded graphic displays the different phases of the flight, plus an additional curve showing the altitude above takeoff level.

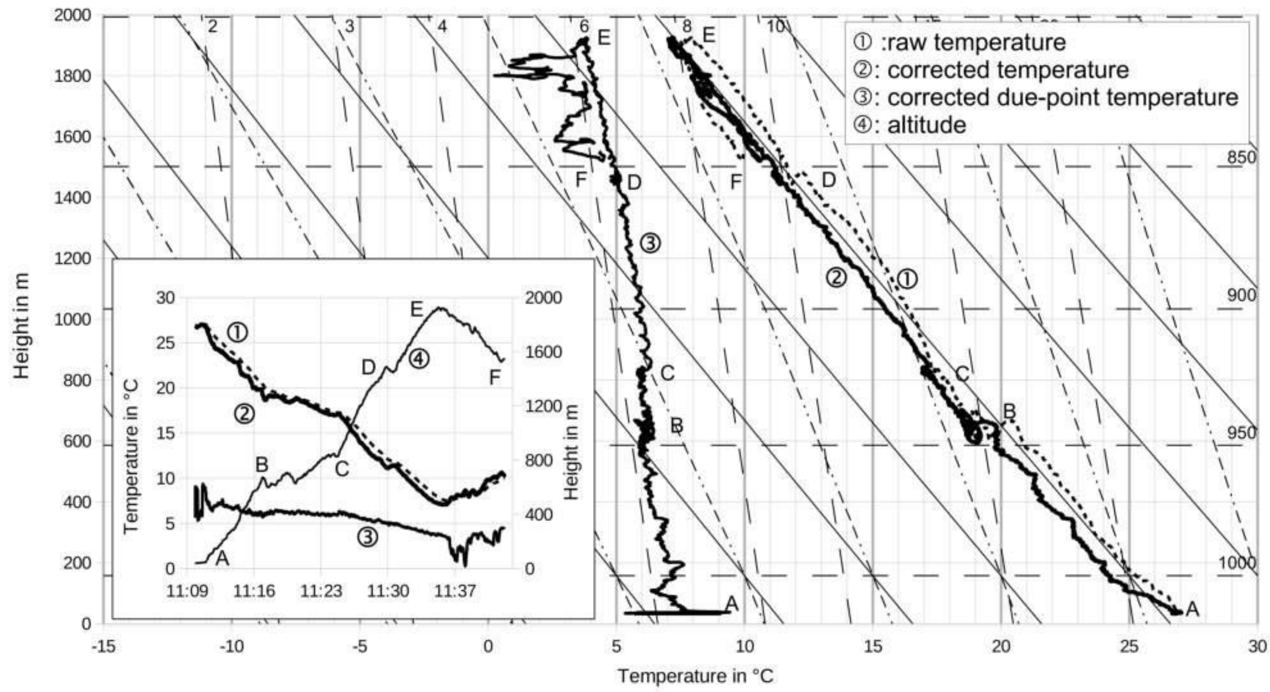

Fig 1: Temperature and due-point temperature during a flight on 14.05.2018.
A: takeoff; B: release; C: entering first thermal; D: entering 2nd thermal; E: leaving thermal; F: entering 3rd thermal

Apparently, the corrected temperature curve aligns on a common line for all phases of the flight.
There is no measurable temperature difference between the thermal and the ambient air. Furthermore, it is obvious that the dew point temperature correlates nicely with the line of constant mixing ratio during the ascent inside the thermal. The mixing ratio is independent of the altitude, which lets us conclude that there was no significant mix with (dryer) ambient air. Any form of entrainment or dilution would have led to a decrease of the mixing ratio with increasing altitude.

During the cruising phase, we measure mostly the humidity of the ambient air, clearly dryer than inside the thermal. Also during that phase of the flight, we experience patches of humid air caused by small thermals in between the main thermals which the pilot decided to use. During the tow phase and at the release of the towrope we experience temperature spikes. This is probably related to the exhaust from the tow plane's combustion engine.

We have only few data points for thermals in low altitude (< 500m GND). Hence, we can't be really sure what the temperature curves look like at those levels. However, we believe there is a positive temperature difference, which is needed to get the thermal off the ground. As the air climbs this temperature difference decreases by the ascend itself as well as by mixing with cooler ambient air. There was one flight, which provided some data to support that assumption. But as the air of the thermal mixes with ambient air we can't treat this as an adiabatic process.

Conclusions

Difference in air-density is the driving force behind thermals. Difference in temperature and humidity is the primary cause of this buoyancy. Extensive measurements over Germany in the summer of 2018 show that humidity is the dominating moving force of the thermals, at least in the upper three quarters between ground and cloud base. In order to recognize this dominance, it is essential either to prevent interfering influences on the temperature measurement or to compensate the measured data mathematically. A faulty temperature measurement can easily lead to the conclusion that the drive of the thermals is wrongly attributed to a, actually not existing, temperature difference. Future measurements will investigate more closely the lower realms where temperature difference is expected to dominate the convective updraft. Furthermore, the algorithms for calculating the thermal strength should also take into account the moisture difference and not solely rely on temperature difference.

References

[And94] Anderson, P. S.: Mechanism for the behavior of hydro active materials used in humidity sensors. In: Journal of Atmospheric and Oceanic Technology, Volume 12, 1995, pp. 662-667

[Bme280] BST-BME280-DS001-12, Final data sheet, rev 1.3, May 3rd, 2016

Measuring the Fine Structure of Thermals

Christof Maul[1,3] and Alfred Ultsch[2,3],

[1] Technische Universität Braunschweig, Germany

[2] Philipps-Universität Marburg, Germany

[3] Akaflieg Frankfurt, Germany

Buoyancy of thermals is a result of density differences between the air masses inside of a thermal and the surrounding air caused by temperature and/or humidity differences.

On board measurements during several flights in arid climate (Namibia) and European climate (Puimoisson) suggest different types of thermals according to either (or both) causes of updraft.

A first classification of different types of thermals types is presented.

Some Common Features of Thermal Waves

Carsten Lindemann

Abstract

Thermal waves of different kind are not so very frequent in Germany, but have been detected in soaring flight with some common features. They can reach more than 2000 m above tops of cumulus clouds, being limited by a stable layer. A mean vertical shear of horizontal wind of 0.005/s or even less starting at cloud top level is sufficient. (FIG. 1) Cloud streets being caused by significant wind can dominate the alignment, but nearly no wind conditions in the convection layer can favor the alignment perpendicular to the upper wind – similar to lee waves. The trigger of thermal waves can be the convection itself or the ability of oscillation of the lower atmosphere due to the Scorer parameter. There can be thermal convection below and wave pattern above without any contact in between. Such situation is sometimes existent of one lower stable layer limiting the thermal convection and another stable layer above for the wave conditions. (FIG.2)

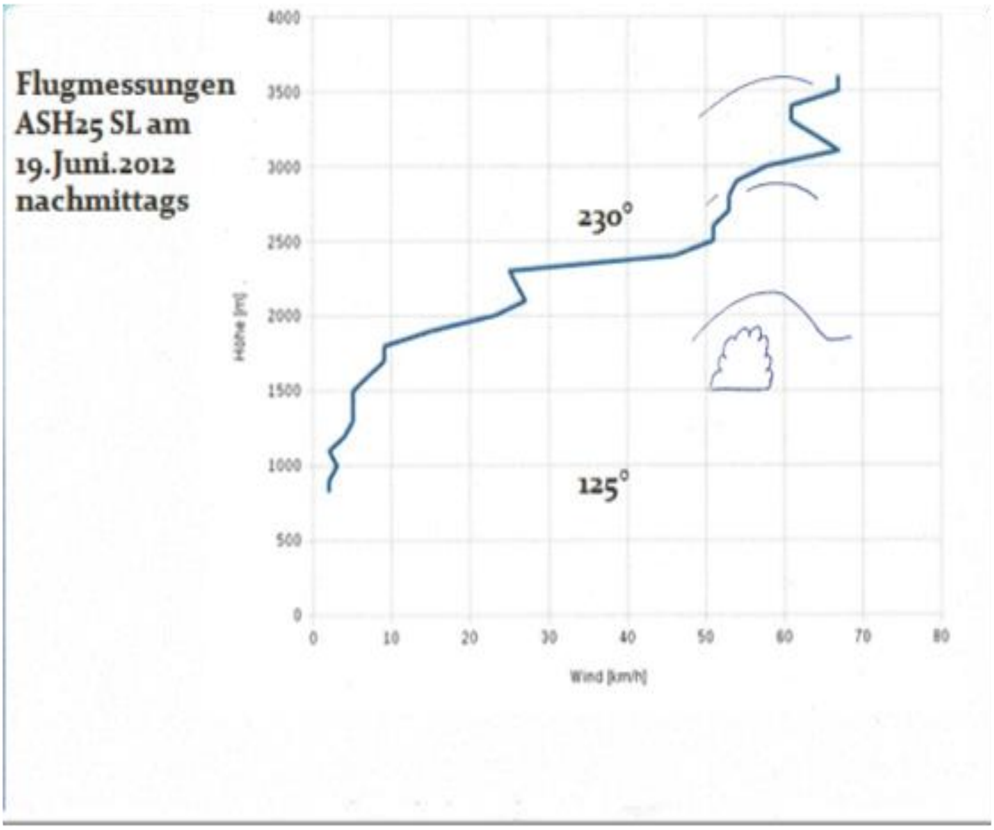

FIG.1 Flight measurements of a classical thermal wave 80 kms SW of Berlin –

Wind shear between 1500 and 3500 m is 0.008/s

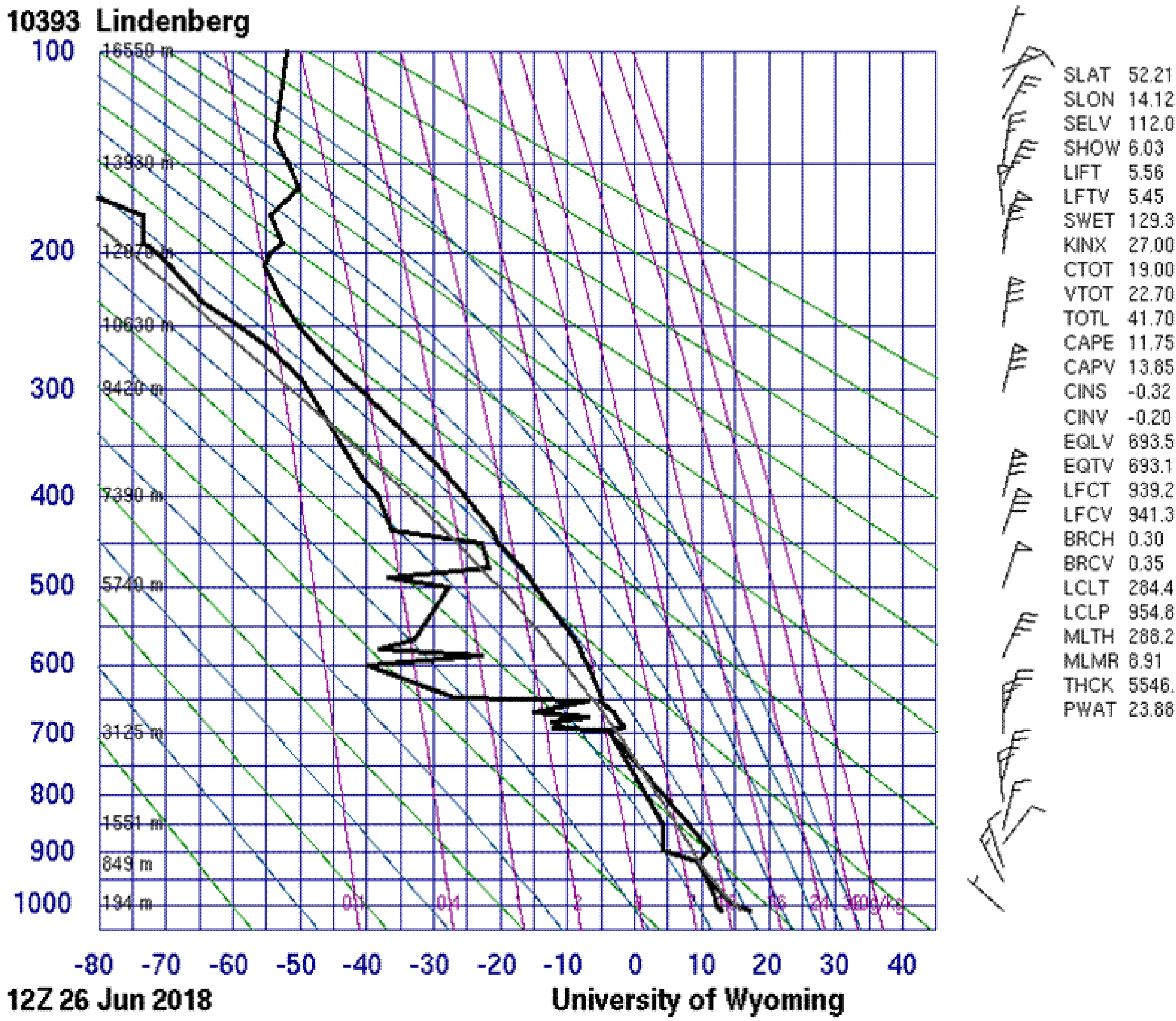

FIG.2 Gravity Waves in mid Troposphere, thermal convection on lowest level –

no thermal wave - wind shear between 1500 and 3500 m is 0.007/s and between 2000 an 5000 m is 0.010/s – Scorer wave parameter satisfied

Diagnostics of Turbulence and Mountain Wave Generation in Aviation Forecasting at the Hungarian Meteorological Service

Péter Salavec[1], André Simon[2], Balázs Szintai[3]

Abstract

The Unit of Aviation Meteorology of the Hungarian Meteorological Service is the Meteorological Watch Office for the Budapest Flight Information Region (LHCC Budapest FIR). Thus, aviation forecasters at the Unit have several regular tasks, including forecasting of turbulence as part of different products: GAMET, AIRMET, SIGMET and LLSIGWX. As the highest mountain in the country does not reach 1500m height AMSL, mountain wave forecasting is officially not provided, however, the Carpathians and Alps often generate mountain waves which can easily extend horizontally over Hungary. In such situations, they are treated as turbulence.

The aviation meteorology website http://aviation.met.hu is operative since 1st November 2016. All products of the Unit are published here. Beside the above mentioned, a section is designed for automatic model forecast outputs. These serve mainly the low-level air traffic (which is constituted mostly by light airplanes, gliders, paragliders, balloons etc.), touristic and sport aviation. The Mountain Wave Gliding subsection is under construction during which several vertical cross-sections and time-height sections will be generated for the wind, vertical velocity, potential and equipotential temperature, relative humidity and the Scorer-parameter (Fig. 1.). Case studies are used to reveal the advantages and general usefulness of the new products which is part of an MSc thesis research at the Eötvös Loránd University.

Another research focuses on turbulence forecasting. This was originally an independent research which aims to improve the description of turbulence by the AROME NWP model (Seity, et al., 2011). This non-hydrostatic model is operative since 2009 and has a 2.5 km horizontal resolution. Its physical parameterization is a 1.5-order closure CBR scheme

[1]*Unit of Aviation Meteorology, Department of Forecasting, Hungarian Meteorological Service*
1. Kitaibel Pál st., Budapest, H-1024, Hungary
[2]*Unit of Storm Warning for Lakes, Department of Forecasting, Hungarian Meteorological Service*
1. Kitaibel Pál st., Budapest, H-1024, Hungary
[3]*Unit of Methodology Development, Department of Informatics and Methodology, Hungarian Meteorological Service*
1. Kitaibel Pál st., Budapest, H-1024, Hungary

(Cuxart, Bougeault, & Redelsperger, 2000) with a prognostic equation for turbulence kinetic energy (TKE). The TKE then can be used to calculate other turbulence-related parameters like eddy-diffusivity, mixing length, etc. These make the model capable to describe turbulence related to mountain waves which wavelength is about 4 km or longer.

The nature of mountain waves implies turbulence generation due to increasing wind shear as well as secondary phenomena (e.g. rotors, wave breaking, etc.). As the spatial scale of these are usually below, or near to, the model resolution, the models often underestimate the turbulence in such situations. Aviation forecasters thus have to give special attention to such situations but the observation of mountain waves is not always easy. This introduces a major hazard for mountain wave gliders. The two originally independent researches converge at this point, as the aim of improving turbulence forecasting, especially in mountain wave situations, is common.

The CBR scheme of the AROME model was originally designed for describing turbulence in the planetary boundary layer, as the turbulent energy transport is significant there. The formulation, however, does not prohibit studying turbulence in the free atmosphere. Occurrence of turbulence can be studied in mountain wave situations with use of TKE and other related parameters. Case studies of significant mountain wave generation and severe windstorms are used in which high TKE values were calculated by the model. The Richardson number (*Ri*), mixing length and other parameters were also studied. It could be shown that the distribution of TKE in the model is highly confined to layers with relatively low static stability and$Ri < 1$. Areas of strong turbulence could be expected near the surface below the wave trough or in the updraft part of the wave (Fig. 2.). One of the strongest events was the severe windstorm of 29 October 2017 when gusts exceeding 100 km/h were recorded in Transdanubia (western part of Hungary). High TKE values (exceeding 10 J/kg) were diagnosed in areas with both high low-level wind shear (below a strong jet) and low static stability (Fig. 3.).

Up to now, it seems that the TKE and other turbulence-related parameters could be successfully used to predict turbulence mainly in the lower troposphere, for General Aviation purposes. However, their added value is uncertain in the free atmosphere and in case of trapped mountain wave situations. For forecasters and pilots, it is also important to provide outputs in understandable form. For instance, we convert the TKE to a corresponding speed of wind perturbation, which can be, for example, compared with the climb rate of the particular aircraft. A method to convert parameter values to the intensity categories defined in ICAO Annex 3 (e.g. EDR) is also under development.

It is concluded that the description of free atmospheric turbulence is rather difficult with the currently available parameterization schemes, as they are mostly designed for describing PBL turbulence. However, mathematical formalism can probably be generalized for the free atmosphere; even the definition of TKE is general on its own. The closure theories introduce constants, which has to be determined, and the aim of PBL measurement campaigns is to collect data for this aim. This requires high frequency, high precision wind and absolute humidity measurements, often together with soil moisture and temperature and surface energy balance (radiation) measurements. The idea of building a separate 1,5-order closure model for TKE in the free atmosphere seems to be useful and is possible using Buckingham-π-theorem and, to be applicable to mountain wave situations, a three-fold Reynolds-decomposition. A measurement campaign in this case has to involve high frequency aircraft measurements in the middle or high troposphere, which is very expensive and difficult to carry out, so this type of measurement campaign is very rare nowadays.

References

Cuxart, J. R., Bougeault, P., & Redelsperger, J.-L. (2000). A turbulence scheme allowing for mesoscale and large-eddy simulations. *Quarterly Journal of the Royal Meteorological Society, 126*(652), 1-30. doi:10.1002/qj.49712656202

Seity, Y., Brousseau, P., Malardel, S., Hello, G., Bénard, P., Bouttier, F., & Masson, V. (2011). The AROME-France Convective-Scale Operational Model. *Mopnthly Weather Review, 139*(3), 976-991. doi:10.1175/2010MWR3425.1

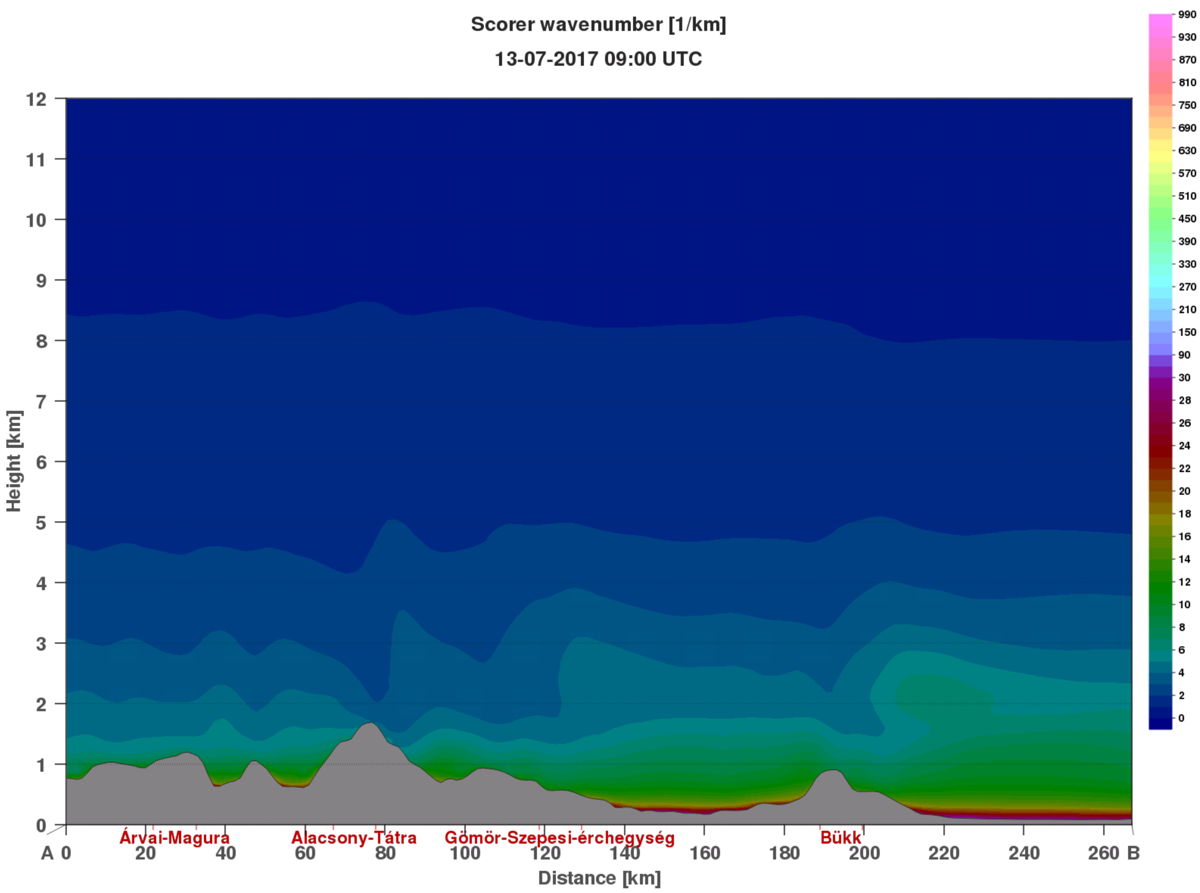

Fig. 1: An example of the mountain wave forecast products: Scorer wavenumber cross-section from Western Carpathians toward Great Plain. High values of the lower 1.5 km suggest possible trapping of waves. Similar time-height sections and cross-sections for several points and sections are under construction.

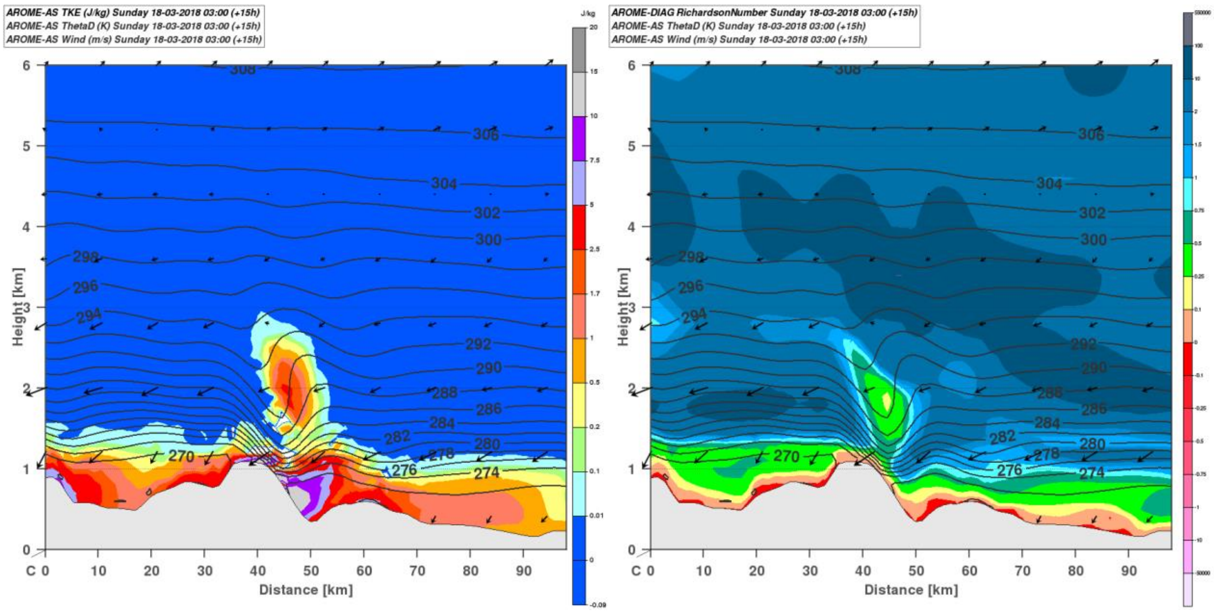

Fig. 2. Left: Vertical cross-section of TKE (J/kg, color shades), potential temperature (K, lines) and wind (arrows) in a situation with strong flow over the Slovak Ore Mountains on 18th March 2018. 03:00 UTC. The products are 15h forecasts of the AROME model. Right: The same, but TKE is replaced by the Richardson number (dimensionless).

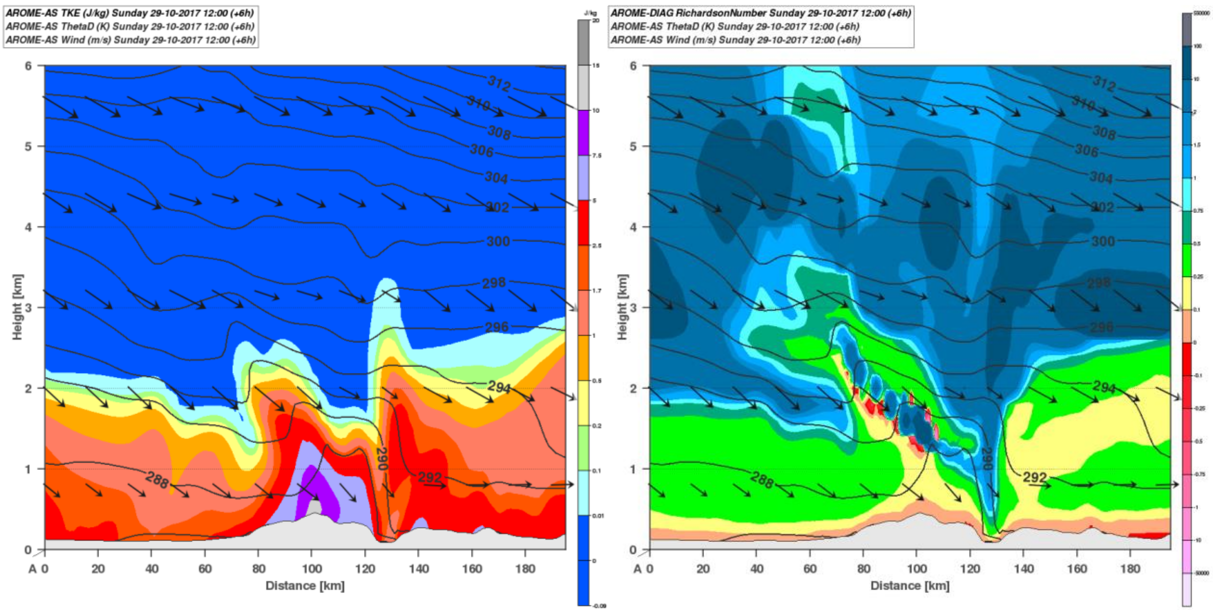

Fig. 3: As in Fig. 1. but in situation with strong turbulence and windstorm behind the cold front on 29th October 2017. at 12:00 UTC (6h forecast of the AROME model). Areas of significant turbulence extend to nearly 2 km height, even in case of Ri somewhat bigger than its critical number (Ri between 0.25 and 1).

Trapped and Vertically Propagating Waves

Timothy Chow
Norwich VT USA
tim_chow@hotmail.com

ABSTRACT

Trapped and vertically propagating waves are two distinct forms of mountain lee waves. To optimally exploit the lift available in these two types of wave the glider pilot must determine what type of wave to expect, how the lift will be distributed, and how they can best exploit the lift to maximize their flight potential. The meteorological conditions, which promotes each type of wave, are discussed and several flights in northern New England (USA) are reviewed as examples.

INTRODUCTION

There are two divisions of the mountain wave: trapped and vertically propagating. Trapped waves assume the form of a series of waves running parallel to the ridge and can extend many miles downwind. They occur when the wind speed increases quickly and stability deceases with altitude (Figure 1). The increasing wind traps the wave against the Earth's surface and the decreasing stability allows most of the energy to propagate downwind.

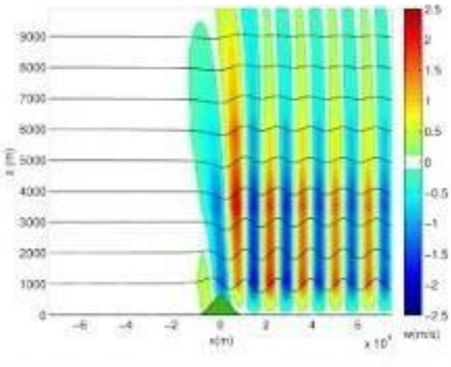

Figure 1: Trapped wave – Streamlines and vertical velocity [Figure 7.9 from Etling, 2014]

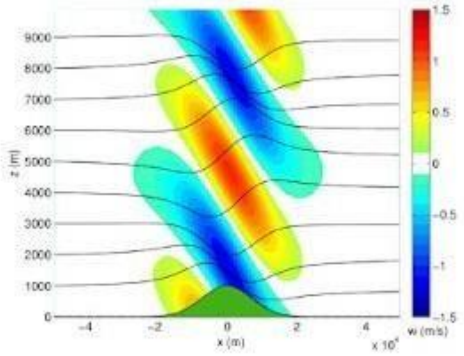

Figure 2: Vertically propagating wave – Streamlines and vertical velocity [Figure 7.7 from Etling, 2014]

With vertically propagating waves (Figure 2), the energy is directed upwards instead of downstream. They occur when the wind speed is relatively constant with increasing altitude, the wavelength is shorter than the base of the mountain and the stability increases with height. Wavelength is proportional to wind speed so, expect vertically propagated waves with low or moderate wind speeds (higher stability also gives shorter wavelengths).

I had a couple of instructive wave flights during the 2018 season that illustrate the trapped and vertically propagating conditions. These flights occurred in northern New England (USA).

TRAPPED WAVE

The first flight (Chow, May 5, 2018) was on May 5th in a trapped wave (Figure 3). I was able to climb to 15,000' directly over Post Mills (Vermont) airport and then travel upwind four wavelengths (53 km) to the Sugarbush (Vermont) airport. At Sugarbush I climbed to 18,000'. From there I was able to cross the spine of the Green Mountains (Mt. Ellen is 4,083’) and climb back up to 18,000' over the flat Champlain Valley. The maximum altitude was limited by airspace restrictions. Pushing ahead two more wave crests put me over the middle of Lake Champlain. From there I could see small cumulus clouds making wave crests all the way to Lake Placid (New York). The wave was generated from the Adirondack Mountains (Mt. Marcy is 5,343’). The day had the ideal amount of clouds. They marked the wave but did not interfere with navigation.

This was a trapped mountain wave. The wave generated by the Green Mountains just upwind of Sugarbush (and Mt. Marcy near Lake Placid) was trapped close to the Earth’s surface as it traveled downwind many cycles to Post Mills. The characteristic wind profile for trapped wave is strong winds and wind speeds increasing with attitude (Figure 4). Note, Figures 4, 6 and 8 are forecasted soundings obtained from http://mtarchive.geol.iastate.edu/ at Iowa State University).

VERTICALLY PROPAGATING WAVE

The second flight (Chow, October 9, 2018) occurred on October 9 during the Mt. Washington Wave Camp in a vertically propagating wave (Figure 5). The vertical wave allowed a climb to over 32,000' (10,000 meters). The wind profile showed relatively lighter winds (about 25 kts at 6,000') and the wind speed did not significantly increase from 5,000' to 50,000' (always below 50 kts, Figure 6). Without the increasing wind (with altitude), forcing the wave along the surface it is free to oscillate into the upper atmosphere. The wavelength was very short with the primary lift over the Mt. Washington Auto Road parking lot.

Another time I (Chow, October 10, 2011) have experienced a vertically propagating wave was on October 10, 2011 (Figure 7). This was probably the best wave day in the history of the modern Mt. Washington Wave Camp. There were many spectacular flights(OLC, October 10, 2011). For example, Rick Roelke (Roelke, October 10, 2011) had a triple-Diamond flight (the three

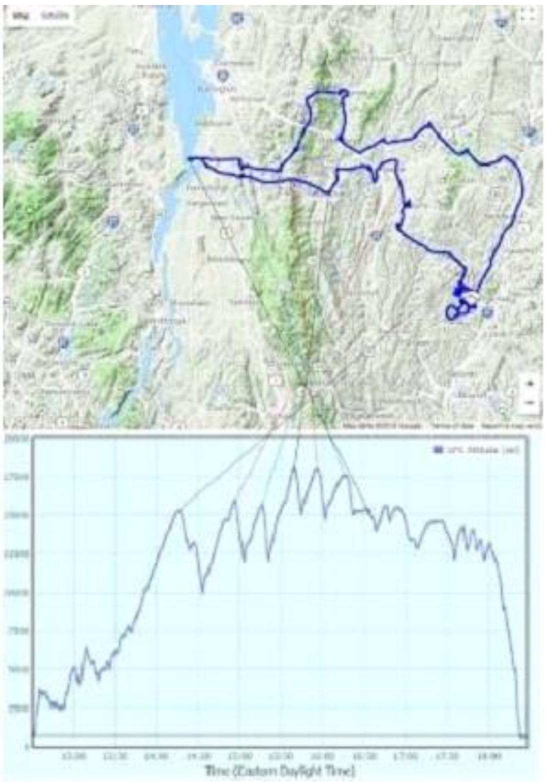

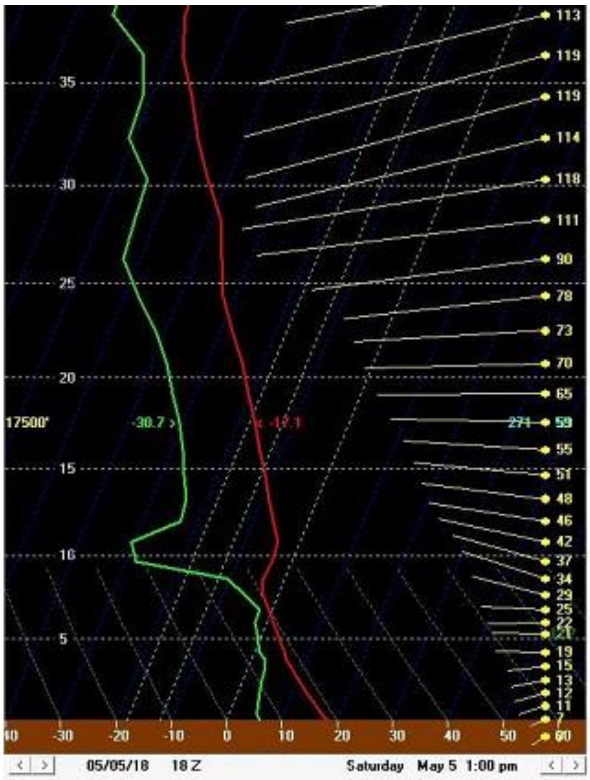

Figure 3: May 5, 2018 Flight - Colored lines show Figure 4: May 5, 2018 NAM forecast sounding valid the peak of each climb.

18GMT (14 EDT) for Burlington Vermont (altitude in feet, wind speed in knots, temperature in Celsius).

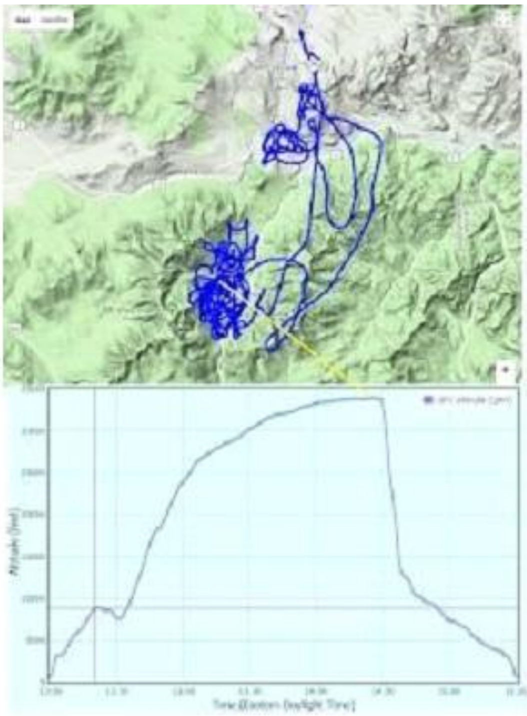

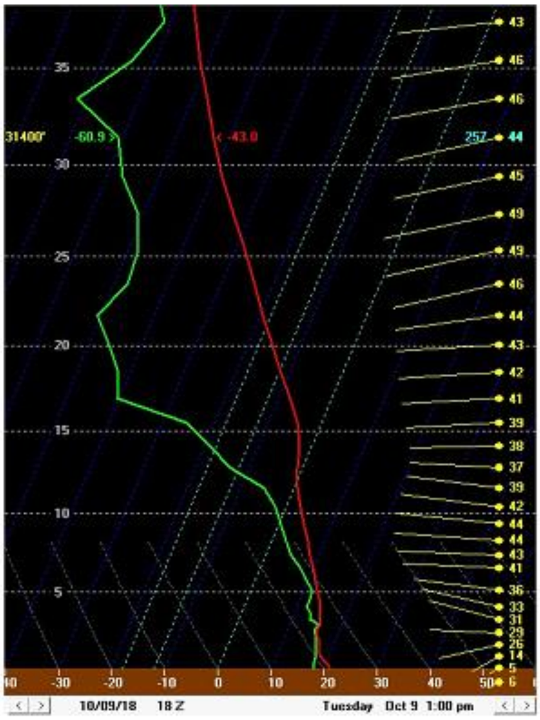

Figure 5: October 9, 2018 flight - Yellow line shows the Figure 6: October 9, 2018 NAM forecast sounding valid 18GMT peak of the climb over the Mt. Washington Auto Road (14 EDT) for Berlin, NH just north of Mt. Washington (altitude in parking lot. feet, wind speed in knots, temperature in Celsius) legs of a Diamond badge in one flight). Evan Ludeman (Ludeman, October 10, 2011) went to 26,000' and then flew 440 km in 8 hours. Jim David (David, October 10, 2011) went over 29,000' (he flew all the way down to Mt. Ascutney (130 km) but failed to find wave lift along the way because the vertical wave did not produce secondary and tertiary lift in the normal places). There were five new Lennie pins (Symons award for flights over 25,000' msl) and many diamond climbs that day.

Figure 7 illustrates my flight on October 10, 2011. It shows the pattern of lift found in the lee of Mt. Washington that can be seen in all the flights from that day. The black arrow shows the location of the top of climb in the primary. It is right over the Auto Road parking lot (very short wavelength). The primary only went to about 13,000'. To go higher I had to drop back to the secondary over the top of Wildcat Mountain (red arrow). In a vertically propagating wave the secondary can go much higher than the primary (see Figure 2). The wind profile from that day (Figure 8) was very similar to October 9, 2018.

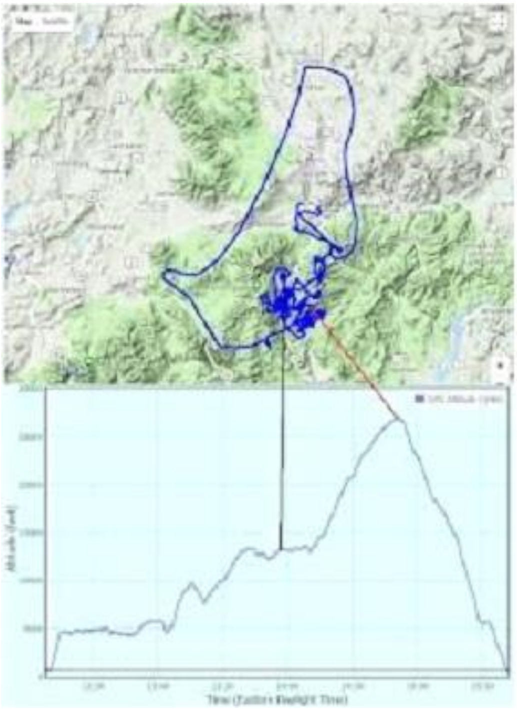

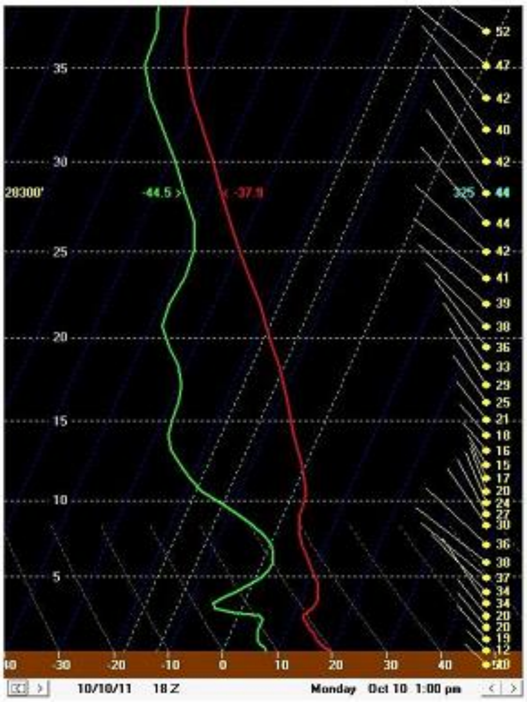

Figure 7: October 10, 2011 – The black arrow marks Figure 8**:** October 10, 2011 NAM forecast sounding valid 18GMT the top of the primary wave. The red arrow shows (13 EST) for Berlin, NH (just north of Mt. Washington) (Altitude the top of the secondary wave. in feet, wind speed in knots, temperature in Celsius)

DISCUSSION

The wind profiles from the NAM model shown in Figures 4, 6 and 8 were checked with actual soundings from the nearest station,

Albany NY. The Albany soundings were generated from the University of Wyoming on-line archive http://weather.uwyo.edu/upperair/sounding.html. The soundings are as follows:

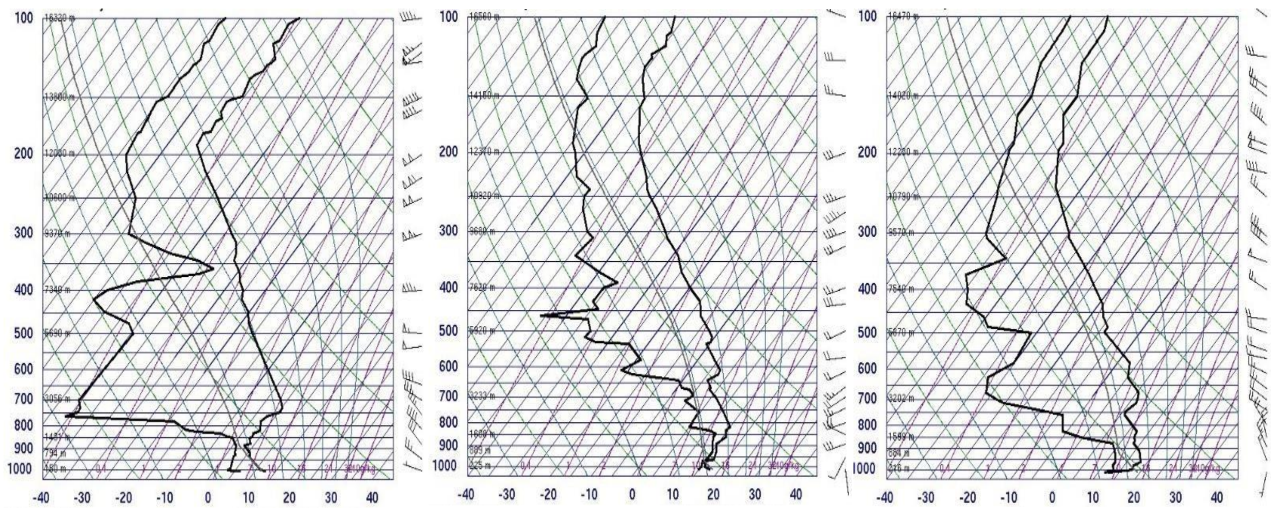

May 5, 2018 Radiosonde data from Albany October 9, 2018 Radiosonde data October 10, 2011 - Radiosonde data NY at 0800 EDT – Note increasing winds from Albany at 0800 EDT - Note the from Albany at 0800 EDT - Note the from 5,000' to 30,000' light consistent winds from 5,000' to light, relatively consistent winds from 50,000'. 5,000' to 50,000'.

The NAM wind profiles are confirmed: The wind profile for the trapped wave (May 5, 2018) shows increasing wind speeds with increasing altitude and the profiles for the vertically propagating waves (Oct 9, 2018 and October 11, 2011) showed relative constant speeds with increasing altitude. Also, note the most stable boundary layer was with the trapped-wave.

CONCLUSIONS

To find wave from areas like Post Mills, Vermont which is 60 km and many wave cycles from the Green Mountains requires a trapped wave. We want **strong** winds and we want the wind **speed** to increase with altitude. The best days at Mt. Washington for long XC and high altitudes flights are going to be those with rare vertically propagating wave. We want lighter winds (short wave length) and we don't want the wind **speeds** to increase **much** with altitude. The highest climbs may be in the secondary.

REFERENCES

Chow, T. (May 5, 2018). https://www.onlinecontest.org/olc-3.0/gliding/flightinfo.html?dsId=6360553

Chow, T. (October 9, 2018). https://www.onlinecontest.org/olc-3.0/gliding/flightinfo.html?dsId=6931357

Chow, T. (October 10, 2011). https://www.onlinecontest.org/olc-3.0/gliding/flightinfo.html?dsId=2146770

Etling, D. (2014). *Atmospheric Gravity Waves and Soaring Flight - Physical principles and practical applications* available for at: https://www.schwerewelle.de/

David, J. (October 10, 2011). https://www.onlinecontest.org/olc-3.0/gliding/flightinfo.html?dsId=2147015

Ludeman, E. (October 10, 2011). https://www.onlinecontest.org/olc-3.0/gliding/flightinfo.html?dsId=2147028

OLC (October 10, 2011). https://www.onlinecontest.org/olc-3.0/gliding/daily.html?sc=1&st=olc&rt=olc&df=&c=US&sp=2011

Roelke, R. (October 10, 2011). https://www.onlinecontest.org/olc-3.0/gliding/flightinfo.html?dsId=2146692

Special Applications of Model Output Statistics (MOS) in Operational Weather Forecasting

Bernd Richter ret. Deutscher Wetterdienst

Model Output Statistics (MOS) is a statistical post-processing procedure that has been published by Glahn and Lowry (1972). It is based on a set* of multiple linear regression equations between predictors and predictands. Predictors are variables from the direct model output (DMO) forecast of a numerical weather prediction (NWP) model, predictands are the variables to be predicted as final forecast.

The multiple linear regression equations are developed on datasets covering the recent few years of NWP model forecast fields and of recent observations. A special feature of the MS-MOS (Meteo Service) presented here is a very sophisticated selection of specially defined predictors in order to describe as much variance of the predictands as possible. Some examples of these specially defined predictors are wind-components perpendicular and parallel to the sea or to a mountain range, simple approximations describing the vorticity of the airflow, indices for the vertical stability and other synoptical parametrizations.

These specially defined predictors showed to be very successful during the past twenty years since MS-MOS has been introduced into the operational forecast section of Deutscher Wetterdienst. Verification results show that operational forecaster can, in general, not improve the forecast quality of MS-MOS. MS-MOS is also in operational use in other MET services, e.g. for spot forecasts in smartphone apps, which can, with respect to numbers, not be accomplished by individual forecasters.

As MOS is based on regression equations with predictors of a specific NWP-model, it corrects for model errors of this NWP-model. As a consequence, MOS has to be developed for each model. Another feature of MOS is the option to predict all variables that have been observed, even if these variables are not element of DMO. This feature is of special importance in aviation forecasts to predict visibility and ceiling. Probability predictands are Important in aviation meteorology and can be forecast by MS-MOS, e.g. PROB (VIS<1000m), (CIG<100ft), (Gust>25KT), (SH), (TS).

MS-MOS is also in operational use to predict non-meteorological parameters (depending on weather, though), e.g. underkeel water clearance for large container vessels coming to Hamburg Harbour with a draught close to the depth of the Elbe river. Forecasts for soaring flight have not been developed yet, but if datasets of observations are available (e.g. max. vertical velocities, top of thermals), this could be subject to development, also for the spatial distribution of these variables.

*set of equations: 15.000 stations worldwide, per station 200 predictands, lead time increment of 3hrs up to 360 hrs, 4 seasons, 250 potential predictors (1-15 accrual predictors)

Glahn, H. R., and D. A. Lowry, 1972: The use of model output statistics (MOS) in objective weather forecasting. *J. Appl. Meteor.*, 11, 1203-1211.